Fully automated production and characterization of ^{64}Cu and proof-of-principle small animal PET imaging using ^{64}Cu-labelled CA XII targeting 6A10 Fab

Luise Fiedler[a]*, Markus Kellner[b], Rosel Oos[a], Guido Böning[a], Sibylle Ziegler[a], Peter Bartenstein[a], Reinhard Zeidler[b][c], Franz Josef Gildehaus[a], Simon Lindner[a]*

[a] L. Fiedler*, R. Oos, PD G. Böning, Prof. S. Ziegler, Prof. P. Bartenstein, Dr. F.J. Gildehaus, Dr. S. Lindner*
Department of Nuclear Medicine,
University Hospital, LMU Munich
Marchioninistrasse 15, 81377 Munich, Germany
E-mail: luise.fiedler@med.uni-muenchen.de and simon.lindner@med.uni-muenchen.de

[b] Dr. M. Kellner, Prof. R. Zeidler
Helmholtz-Zentrum München, German Research Center for Environmental Health, Research Group Gene Vectors
Marchioninistrasse 25, 81377 Munich, Germany

[c] Prof. R. Zeidler
Department of Otorhinolaryngology,
University Hospital, LMU Munich
Marchioninistrasse 15, 81377 Munich, Germany

Abstract: ^{64}Cu is a cyclotron-produced radionuclide which offers, due to its characteristic decay scheme the possibility to combine PET investigations with radiotherapy. We evaluated the Alceo system from Comecer SpA to automatically produce ^{64}Cu for radiolabelling purposes. We established a ^{64}Cu production routine with high yields and radionuclide purity in combination with excellent operator radiation protection. The carbonic anhydrase XII targeting 6A10 antibody fab fragment was successfully radiolabelled with the produced ^{64}Cu and proof of principle small animal PET experiments on mice bearing glioma xenografts were performed. We obtained a high tumor-to-contralateral muscle ratio, which encourages further *in vivo* investigations of the radioconjugate regarding a possible application in diagnostic tumor imaging.

Introduction

As a powerful non-invasive imaging tool, positron emission tomography (PET) offers the possibility to visualize and monitor biochemical and physiological functions as well as pathophysiological processes *in vivo*. To investigate fast molecular distribution and accumulation characteristics, short-lived PET-radionuclides such as ^{11}C ($T_{1/2}$ = 20.4 min), ^{68}Ga ($T_{1/2}$ = 67.7 min) and ^{18}F ($T_{1/2}$ = 109.8 min) are commonly used [1-6]. [^{18}F]FDG for instance is a radiolabelled glucose molecule with fast tumor uptake characteristics, and one of the most prominent tracers in the field of tumor imaging [6-7]. Radionuclides with longer half-lifes, such as ^{89}Zr ($T_{1/2}$ = 3.27 days) and ^{124}I ($T_{1/2}$ = 4.18 days), are needed to image molecules with slower biochemical processes and longer blood availability, like antibodies [8-9]. Fab (fragment antigen binding) fragments of antibodies on the other hand, have a shorter bioavailability than full-length antibodies, but much longer availability than small molecules as glucose [10-12]. Radiolabelling such molecules with an intermediate half-life PET-nuclide like ^{64}Cu ($T_{1/2}$ = 12.7 h) might therefore be promising. Furthermore, ^{64}Cu decay includes in addition to β^+ and electron capture a significant β^- component (probability of 39.0 (3)%) [13-15]. Thus, the combination of PET imaging with radiotherapy may be feasible, which is not the case for ^{124}I and ^{89}Zr [16-19].

Various kinds of molecules have so far been radiolabelled with ^{64}Cu to investigate possible PET applications against a wide range of diseases. One of the most common ^{64}Cu-radiolabelling methods is based on using a chelating agent to bind the radioactive metal to the carrier molecule. Copper offers well-established coordination chemistry which allows the use of various chelators, for instance DiamSar, NOTA, NODA-GA, PCTA and their derivatives [20-21]. Using chelator-conjugated antibodies, ^{64}Cu has been investigated in studies against pancreatic cancer [22], malign lymphoma [23], breast cancer [24] and CA IX expressing malign tissue [25]. Antibody fragments (Fab and F(ab)$_2$), also radiolabelled with ^{64}Cu via chelators, have currently used in studies against ovarian cancer [26], breast cancer [26-27], and head and neck cancer [28]. Chelator molecules are further used to bind ^{64}Cu to peptides, for example RGD$_2$-BBN heterotrimers against prostate cancer [29] and RGD peptides against gliomas [30]. Chelator-conjugating is even used to radiolabel nanoparticles [31] and liposomes for breast cancer diagnosis [32]. Copper - labelled complexing agents such as ATSM or some bifunctional chelators are further investigated for the use as diagnosis agent against hypoxia [33-34] and Alzheimer´s disease [35-36], respectively. Since chelators might change the pharmacokinetics and binding ability of the conjugated molecule, the development of chelator-free radiolabelling strategies is interesting. Using nanoparticles based on gallic acid is one way to ensure chelator-free radiolabelling, since the containing phenol groups strongly interact with the ^{64}Cu [37-39]. Promising preclinical results of such approaches have already been reported in studies against breast cancer [37-38, 40]. A further method to generate ^{64}Cu-labelled structures is the use of radioactively doped starting material. As a result, the radionuclide is embedded in the structure´s matrix, as for example ^{64}Cu-containing quantum dots which are under investigation for PET-studies against gliomas [41]. Furthermore, structures like liposomes or micelles or even nanoparticles can be used to encapsulate ^{64}Cu-linked molecules which might be useful to influence the molecules properties, for instance increasing its hydrophilic properties [39, 42]. Due to this wide range of promising applications for ^{64}Cu, establishing a production routine is further investigated in this study.

The cyclotron production of ^{64}Cu via the ^{64}Ni(p,n)^{64}Cu reaction has already been extensively investigated [18-19, 43]. Several groups have established ^{64}Cu production routines so far, but mostly with individual custom-made, semi-automated processes and equipment [19, 44-47]. Comecer SpA (Castel Bolognese, Italy) developed an automatic setup, the so-called Alceo modules to cover all processes regarding ^{64}Cu production: electrochemical fabrication of the ^{64}Ni target, cyclotron irradiation and subsequent dissolution of the target, purification and final preparation of the ^{64}Cu product. All procedures can be performed automatically without manual intervention, which ensures a high level of radiation protection for the operator. Matarrese et al. [48] firstly introduced these modules but used an individual modified electrochemical cell. Our study is now focussed on establishing a ^{64}Cu routine production with the unmodified, commercially avail-

able 1st generation Alceo modules (see Figure 1) to perform preliminary PET imaging experiments.

The Alceo setup consists of the PRF (purification), the EDS (electrodeposition/ dissolution/ transfer/ storage) and the PTS (irradiation/ cooling) unit. To prepare the irradiation target, a ^{64}Ni solution circulates between the PRF and the electrochemical cell in the EDS module. A main part of the electrochemical cell is the so-called shuttle, which is a cylindrical, hollow aluminium device (height 35 mm, diameter 28 mm) with an integrated platinum beaker. The ground area of this beaker is used as backing for the ^{64}Ni electrodeposition. The lid of the electrochemical cell equipped with a platinum rod anode, is closed above the shuttle which is placed on the gold foiled brass cathode beneath (see Figure 2). Through a tube system, the shuttle is automatically transferred to the PTS module, which is installed on the in-house biomedical cyclotron and positioned in the beamline. Cooling of the shuttle backing and the nickel target during irradiation is maintained using water and helium, respectively.
The shuttle is delivered back to the EDS unit, and the irradiated target is dissolved using the circularly arranged capillaries between EDS and PRF. The target solution is purified with anion exchange chromatography [49] in the PRF. Recovered nickel can be processed for the repeated use as target material. The purified $^{64}CuCl_2$ is sent to the TADDEO module (Comecer SpA, Castel Bolognese, Italy) for volume reduction (Figure 1 – D).

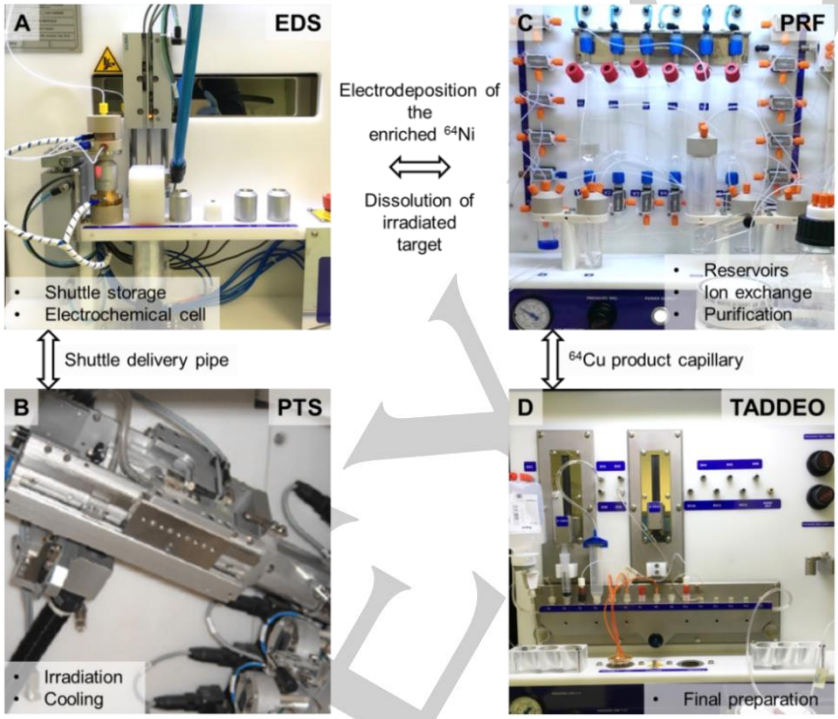

Figure 1: Modular setup of the Alceo system: The Shuttle is transported between the EDS (A) and PTS (B) via a delivery pipe, EDS (A) and PRF (C) are connected by capillaries to enable the circulating fluid transport and the final product is transferred from the PRF (C) through capillaries to the TADDEO module (D) for final processing.

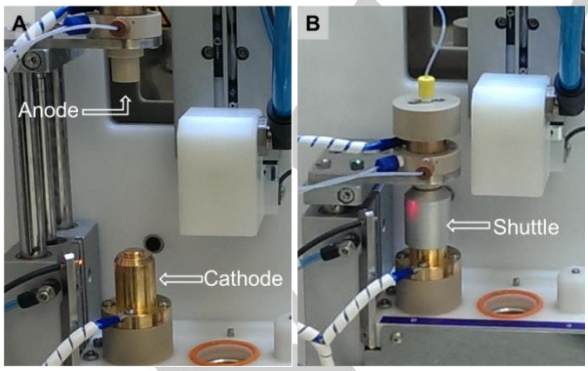

Figure 2: Electrochemical cell of the EDS module. A: open cell with marked positions of anode and cathode. B: Shuttle in position for electrodeposition and dissolution with closed electrochemical cell.

The produced ^{64}Cu was further characterized, used for radiolabelling experiments, and first *in vivo* small animal PET imaging experiments were performed. Therefore, the fab fragment of the new 6A10 antibody (6A10 Fab) was used, which binds highly specific to carbonic anhydrase XII (CA XII)[50-51]. CA XII is a membrane enzyme, which catalyses the generation of bicarbonates for buffer purposes in cells, which are covering their high energy demands by extensive anaerobic glycolysis [50-51]. This enzyme is expressed on various aggressively growing cancer cells [52-53], such as renal carcinoma [54-56], breast cancer [57], ovarian tumors [58] and gliomas [59]. The 6A10 Fab has already been radiolabelled with ^{177}Lu and investigated for the potential use as a radiotherapy agent against glioma recurrences [60]. Further applications as a diagnostic tracer, radiolabelled with the PET-nuclide ^{64}Cu, is now considered to extend the use of this biomolecule for tumor imaging.

Next to the establishment of an automated Cu production with the Alceo setup, the aim of our study was to evaluate the possibility to generate a ^{64}Cu-labelled 6A10 Fab for proof-of-principle PET experiments on mice, bearing CA XII expressing tumor xenografts.

Results and Discussion

Target preparation and irradiation

Enriched ^{64}Ni is electrochemically deposited from an aqueous $Ni(SO_4)_2$ solution in a dynamic cycle. In comparison to other groups, who used static electrochemical cells for nickel target deposition [19, 44-45, 61-62], the Alceo setup utilizes the dynamic deposition method, in which the shuttle is part of the electrochemical cell and the nickel is deposited directly on the shuttle´s platinum beaker. This method prevents the accumulation of hydrogen at the cathode, which has been reported to disturb the deposition process when using static setups [48, 63]. To successfully produce a nickel target for irradiation, the flow of the electrolyte solution needs to be adjusted very accurately to 1.2 – 1.4 ml/min. In this flow range, typical electrodeposition yields of up to 96% were reached. When using flows higher than 1.4 ml/min, the yields radically decreased. Recovery and re-electrodeposition of already irradiated nickel material was accomplished with yields of up to 90%. The generated deposit (see Figure 3-B) was conically shaped, with an area of 7 mm in diameter, an increasing thickness in the middle and a rough, pitted surface. This appearance was most likely caused by the geometry of the electrochemical cell, as the anode is a platinum rod and the cathode a round shaped platinum surface. The anode is positioned centrically above the cathode, which results in an increased deposition rate in the middle. Since the target gets very pointy and brittle on the tip when too much material is deposited, nickel amounts above 85 mg are not usable for further irradiation experiments.

A paper burn test was performed to determine the beam position on the shuttle required to effectively irradiate the nickel target. For that reason, a shuttle was equipped with a paper and irradiated for a short time. In Figure 3, images A and B show the beam position on the burned paper and a representative nickel target. The cross in both figures indicates the centre of the shuttle, where both, ^{64}Ni and proton beam are located. This confirmed that the beam successfully hits the target during irradiation.

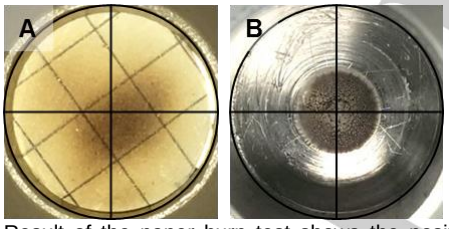

Figure 3: Result of the paper burn test shows the position of the beam on the shuttle (A) while B shows a ^{64}Ni-plating on the shuttle´s platinum beaker.

The beam energy was varied through the installation of aluminium foils with different thicknesses in the beam line. According to the ^{64}Ni(p,n)^{64}Cu cross section, the highest nuclear reaction yield can be expected at 11 MeV proton beam energy [64-65]. However, we observed an overall decreasing activity yield in correlation with the decreasing beam voltage. Proton energies of 11, 13.2 and 14.5 MeV resulted in average yields of 0.25 ± 0.15, 0.44 ± 0.14 and 0.72 ± 0.20 MBq/µA/h/mgNi, respectively. This can be explained with a decreased proton flux hitting the target with increasing degrader foil thickness. Table 1 contains a summary of 16 representative ^{64}Cu production runs with the corresponding amounts of used ^{64}Ni, irradiation parameter, and radioactive yields.

When comparing batches with similar amounts of nickel (B1 and B3, B5 and B7, B8 and B9), the yielded activity at the end of bombardment (EOB) was improved by elevating the beam current and duration. Increasing the amount of nickel target but using constant beam parameters (B12 and B13, B10 and B11, B16 and B15) also resulted in improved yields. Higher nickel amounts cannot be deposited and longer irradiation times or higher currents are limited due to technical restrictions. Nevertheless, significant yield deviation was observed, even though similar nickel amounts and equal beam parameters were used (B13 and B15, B12 and B14). These variances are most likely due to an uneven quality of the nickel target, caused by an unreliable electrodeposition process. The Alceo setup is characterized by a very long capillary circuit, which is used in different steps of the ^{64}Cu production. This can cause ionic cross contaminations, which might disturb the electrochemistry process and can lead to irregular nickel deposition. Additionally, the pre-installed membrane pump is not able to establish a constant flow of the solution. Thus, to produce a reliable ^{64}Ni target and consequently a predictable irradiation yield, modification of the pump and the electrochemical cycle is highly recommended to increase the irradiation output.

Table 1: List of 16 ^{64}Cu production runs with the sample IDs, the corresponding amounts of ^{64}Ni, beam parameters and resulting yields, decay corrected to the end of bombardment (EOB).

ID	^{64}Ni [mg]	Beam parameters		Yield EOB	
		[MeV]	[µA*h]	[MBq]	[MBq/µA/h/mgNi]
B1	46.9	14.5	18	660	0.72 ± 0.20
B2	58.0	14.5	60	2362	
B3	50.6	14.5	85	4443	
B4	41.0	14.5	100	3604	
B5	84.5	14.5	57	3100	
B6	82.0	14.5	75	2509	
B7	83.5	14.5	100	5389	
B8	85.3	11.0	100	941	0.25 ± 0.15
B9	78.5	11.0	150	1702	
B10	24.0	11.0	150	1532	
B11	39.7	11.0	150	2005	
B12	23.0	13.2	150	1826	0.44 ± 0.14
B13	42.0	13.2	150	2394	
B14	26.0	13.2	150	976	
B15	42.6	13.2	150	3969	
B16	35.0	13.2	150	2118	

Characterization

The irradiated target was dissolved in HCl and the ^{64}Cu was separated from nickel target material and irradiation by-products using anion exchange chromatography. With a final volume of 9 ml, the $^{64}CuCl_2$ was not suitable for radiolabelling purposes, so the product was evaporated to dryness and re-dissolved in HCl (400 µl; 0.1 M) using the TADDEO module. The final $^{64}CuCl_2$ had a pH of approx. 0.4 at the end of preparation (EOP). A half-life of 12.7 h ± 0.5 h was confirmed via dose calibrator measurement. The identity of the produced ^{64}Cu was verified by gamma spectroscopy (see Figure 4). Next to the 511 keV peak, the characteristic γ – peak of ^{64}Cu at 1345 keV was identified. The radionuclide purity was calculated to be > 99% (EOP).

When irradiating enriched ^{64}Ni with protons, the formation of radionuclide by-products has been reported previously [19, 45-46, 66]. Due to the limited purity of enriched ^{64}Ni (< 99.32% purity), some impurities are expectable. To eliminate short-lived copper isotopes, anion exchange purification of the product was performed after an overnight decay (approx. 12 h), which resulted in excellent radionuclide purity at the end of preparation. All purification fractions were analysed with gamma spectroscopy and the overall contents of radionuclides were quantified. Table 2 shows the resulting contents of n = 11 separations in atomic percent (At%), decay corrected to EOB.

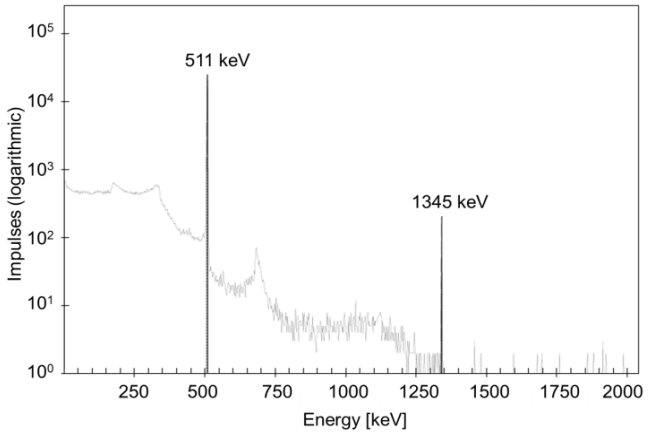

Figure 4: Exemplary gamma spectrum of the produced ^{64}Cu with the annihilation peak (511 keV) and the copper specific γ – peak at 1345 keV.

Table 2: Average amounts of irradiation products in atomic percent (At%) at EOB (n=11). Nuclides, which were not detected, are declared as n. d. (not detectable). Gamma spectrometry measurements were performed 10-12 h post EOB.

Element	Isotope	Half-Life	Mean At% at EOB (n = 11)
Cobalt	55	17.5 h	0.03 ± 0.10
	57	271.8 d	0.004 ± 0.014
	61	1.7 h	1.4 ± 3.4
Copper	60	23.7 min	n. d.
	61	3.4 h	n. d.
	62	9.7 min	n. d.
	64	12.7 h	98.5 ± 3.4

The cobalt isotopes ^{55}Co, ^{57}Co and ^{61}Co were identified with contents of 0.03 ± 0.10, 0.004 ± 0.014 and 1.4 ± 3.4 At%, respectively. The amount of ^{64}Cu was determined to be 98.5 ± 3.4 At%. Radionuclides with short half-lifes, such as $^{60\text{-}62}$Cu, were not detected in the examined sample. This supports the implementation of a 12 h time interval between EOB and EOP for elimination of any short-lived isotopes.

The molar activity (A_m) of the produced $^{64}CuCl_2$ was determined by titration with the chelator 1,4,8,11-Tetraazacyclotetradecane-1,4,8,11-tetraacetic acid (TETA)[19]. To do so, aliquots of TETA in different concentrations were radiolabelled with ^{64}Cu and the radioactive yield was determined with radio-TLC. Due to an equimolar reaction between metal and chelator, the molar activity in Becquerel per mole can be calculated. Non-radioactive metallic ion contaminations would compete with the ^{64}Cu to complex with TETA, so this method determines the effective molar activity (eff. A_m) of the entire $^{64}CuCl_2$ product rather than the theoretical activity per mole ^{64}Cu. To determine the theoretical A_m, a direct method such as mass spectrometry techniques is recommendable [44-45]. Since the eff. A_m is decisive for radiolabelling purposes we focused on the TETA titration method in this study.

Improving the eff. A_m was accomplished by changing the solvent for cleaning of all the modules reservoirs and capillaries prior to ^{64}Cu production. We firstly used only Tracepur® water (≤ 1.0 ppb Cu; ≤ 1.0 ppb Fe) and switched during development to a two-step method, which includes pre-cleaning with Tracepur® water and final rinsing with Ultrapur® water (≤ 0.1 ppb Cu; ≤ 0.3 ppb Fe). To monitor the rinsing efficiency, diluted aliquots of decayed $^{64}CuCl_2$ batches were analysed with ICP-OES for metallic contaminations of Co, Cr, Mn, Ni, Zn, Cu and Fe. Metal contents of significance were found for Cu, Fe, Ni and Zn, and are plotted in Figure 5 in correlation with the determined effective molar activity.

B6 and B7 show the results of a system, which was rinsed with Tracepur® water using a small anion exchange column (3 g resin) for separation. In both batches, remarkable high amounts of Fe and Zn were detected. The amount of resin was increased up to 9 g in B10 and B13, while rinsing was still carried out with Tracepur® water, resulting in decreased Fe and Zn contents.

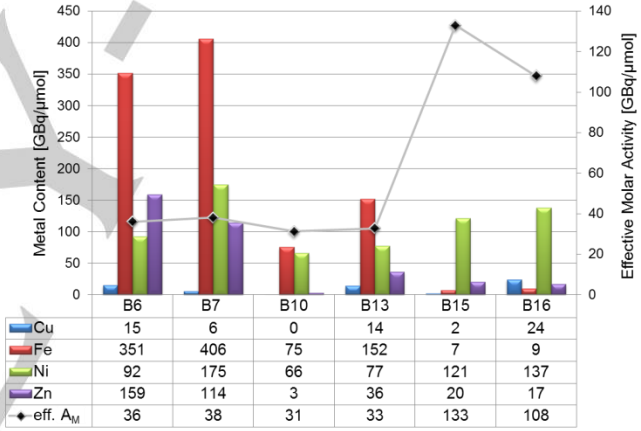

Figure 5: A representative comparison of the contents of non-radioactive metals [µg/ml] and the corresponding molar activity (A_m) [GBq/µmol].

Finally, cleaning of all production relevant lines and cycles was performed with Ultrapur® water, leading to a decreased content of Fe in B15 and B16. Simultaneously, a significant improvement of the eff. A_m was reached using high purity water for cleaning (120.5 ± 17.7 GBq/µmol in B15 and B16 versus 34.5 ± 3.1 GBq/µmol in B6, B7, B10 and B13).Varying amounts of Cu and Ni were detected over all batches.

The amount of determined nickel in the product does not correlate with improvements made for purification and rinsing. We therefore assume that the majority of the nickel originates from the nickel target. Minor amounts of non-radioactive Ni and Zn can be attributed to the ^{64}Cu decay, since it is characterized by 39.0 (3)% β^- decay to ^{64}Zn ground state and 17.86 (14)% β^+ and 42.6 (5)% electron capture decay to ^{64}Ni ground state [13-15]. Co, Cr and Mn were not found in significant amounts.

An optimized molar activity of ^{64}Cu is an important prerequisite for imaging purposes. Using different technical setups, processing methods and irradiation parameters, a wide range of possible molar activities has been published so far. Table 3 shows a comparison between the results presented in this study

and previously published molar activities of other groups. With up to 133 GBq/µmol our method generates moderate values, higher than those reported by Jeffery et al.[45], Matarrese et al.[48] and Obata et al.[62] but lower than those achieved by Avila-Rodriguez et al.[46], McCarthy et al.[19], Ohya et al.[67] and Thieme et al.[44]. Our results can best be compared with those of Matarrese et al.[48], who also worked with the Alceo modules. They reported an effective molar activity of 81.4 ± 48.1 GBq/µmol which was moderately improved to maximum 133 GBq/µmol in this study.

Table 3: Comparison of the molar activities reported in previous studies and in this study, in correlation with the used measurement methods.

Author	Molar activity [GBq/µmol]	Measurement method
Ohya et al. 2016 [67]	1170 ± 1170	ICP-MS
Avila-Rodriguez et al. 2007 [46]	696 ± 122	Titration with TETA
Thieme et al. 2012 [44]	1072 ± 420	ICP-MS
McCarthy et al. 1997 [19]	Up to 733	Titration with TETA
Current study	Up to 133	Titration with TETA
Obata et al. 2003 [62]	118 ± 67	Titration & HPLC with ATSM
Jeffery et al. 2012 [45]	89 ± 37	ICP-MS
Matarrese et al. 2010 [48]	81 ± 48	HPLC

Limitations of the Alceo modules

By using the first generation Alceo modules an automatic production of ^{64}Cu can be established. However, some improvements might be recommendable to further optimize the process reproducibility and the molar activity of the ^{64}Cu product. The modules are equipped with very long capillary circuits for all production steps and the same lines are used for nickel electrodeposition and dissolving prior and post irradiation. This might result in metal ion cross contaminations, which have to be removed by extensive rinsing procedures. A better way to diminish problems associated to those cross contaminations would be to strictly separate the two cycles and to significantly shorten the fluid pathways. Furthermore, a setup based on disposable kits would even guarantee a production which is free of any contaminations.

An improved reproducibility regarding the electroplating process can further be reached by installing a pump with a more stable performance since the pre-installed device shows unequal pump velocity over a long operating time.

The initially produced $^{64}CuCl_2$ is so far available in 9 ml which results in a volume-concentration too low for radiolabelling purposes. In this study, the TADDEO module had to be used for volume reduction. With an integrated solution, for example a pre-installed heating device for evaporation, the Alceo setup would enable a convenient production outcome of labelling-suitable ^{64}Cu.

Radiolabelling and PET imaging

The 6A10 Fab, conjugated with *p*-NCS-benzyl-NODA-GA, was radiolabelled with ^{64}Cu and purified with a nap-5 column (GE Healthcare, Munich, Germany). The radiochemical purity of the product was determined with radio-TLC to be > 93%. In 5 synthesis runs, we reached a final specific activity of the radiolabelled compound of 208.6 ± 49.7 MBq/mg. A female SCID-mouse, bearing a glioma xenograft on the right shoulder (approx. 370 mm^2) was injected with 14.7 MBq of the conjugate via a tail vein catheter and scanned with small animal PET. The image is depicted in Figure 6. The tumor-to-contralateral muscle ratio was calculated to be 12.

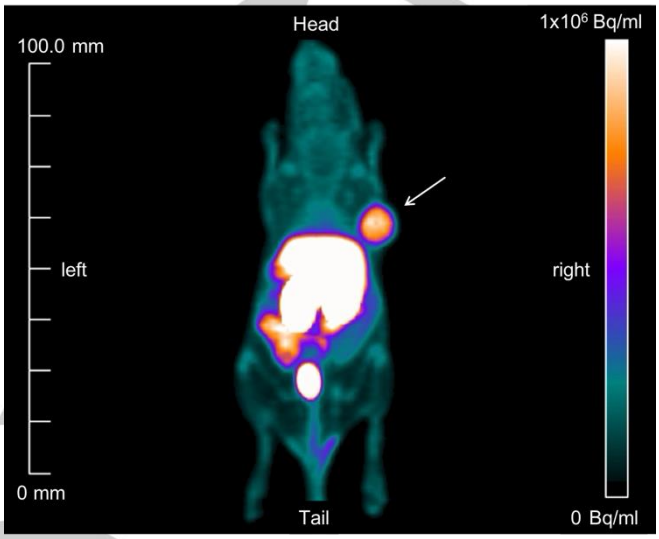

Figure 6: PET image of a mouse, scanned 4 h after the injection of 14.7 MBq of the radioconjugate. The tumor xenograft on the right shoulder is indicated with a white arrow.

The image also shows activity accumulation in organs such as kidney, liver, bladder, spleen and the intestines. According to our previous work [60], this accumulation pattern can be expected, since the metabolism of proteins with a molecular size like a fab fragment (approx. 55 kDa) is dominated by kidney and liver. The calculated tumor – to – contralateral muscle ratio of 12 is notably high for a systemically applied fab fragment, since Fabs undergo fast degradation processes and are therefore much more short-lived in the blood than full-length antibodies [10-12]. This encourages further studies regarding the *in vivo* behaviour of this ^{64}Cu - labelled compound for diagnostic imaging of CA XII expressing tumors.

Conclusions

The Comecer Alceo modules offer the possibility to produce ^{64}Cu in good radioactive yields, high radiochemical purity, and good effective molar activity for radiolabelling of biomolecules. Due to the high grade of automatization an excellent radiation protection for the operator can be expected. Labelling of the 6A10 antibody fab fragment and proof of principle small animal PET experiments were accomplished and showed promising imaging results.

Further studies are considered to investigate the *in vitro* and *in vivo* characteristics of the ^{64}Cu-labelled 6A10 Fab in regard to a possible diagnostic application against CA XII expressing tumors.

Experimental Section

Unless otherwise mentioned, all chemicals and expendable items were purchased from Sigma Aldrich (Taufkirchen, Germany), Carl Roth (Karlsruhe, Germany), or Eppendorf (Hamburg, Germany).
All glassware and capillaries are routinely cleaned prior to production with HNO_3 (2 M), rinsed with water and dried with nitrogen. During the evaluation process in this work, the purity grade of the used water was continuously refined.

Target Preparation
The electrolyte bath was prepared according to McCarthy et al.[19]. The enriched ^{64}Ni (20 – 90 mg, <99.32% purity, (Chemotrade Chemiehandelsgesellschaft mbH, Düsseldorf, Germany) was dissolved in HNO_3 (2 ml, 6 M), evaporated to dryness, redissolved in H_2SO_4 (300 µl, concentrated), diluted with H_2O (2 ml), evaporated to almost dryness and diluted with H_2O (5 ml). The pH was adjusted at approx. 9 with NH_3 and $(NH_4)_2SO_4$ (0.3 mg) and H_2O (2 ml) was added to a final volume of 8 - 9 ml.
Nickel deposition on the shuttle occurred under constant circulation of the solution with 1.2 – 1.4 ml/min, at 2.6 V and a current between 0 – 30 µA, depending on the amount of nickel remaining in the solution. After 20 – 24 h, the solution turned colourless, which indicates the complete nickel deposition. By weighting the shuttle before and after electrodeposition, the amount of deposited nickel was determined. The circulation cycle and the plated nickel was rinsed with H_2O and dried with nitrogen.

Irradiation
For irradiation a PETtrace 800 series cyclotron from GE Healthcare (Uppsala, Sweden) was used. Confirmation of the correct shuttle position in the beam line was obtained by a paper burn test. For that purpose, a shuttle was equipped with a paper and irradiated for 16 s with 5 µA at 13.2 MeV.
Several irradiation conditions were tested. The initial 16 MeV beam was degraded by different aluminium foils. Using 320, 500 and 820 µm foils resulted in beam voltages of 14.5, 13.2 and 11 MeV, respectively [68]. The irradiation took up to 5 h and current values between 20 – 30 µA were tested. The temperature range of cooling water and helium was set to be at approx. 20 ± 5 °C.

Purification and preparation of ^{64}Cu
After an overnight decay, the irradiated target was dissolved with HCl (5 ml, 6 M) at 90 °C shuttle temperature over 1 h. A BioRad Econo-Column with AG1-X8 chloride form resin (200-400 mesh, BioRad, Hercules, California, USA) was loaded with the solution. In three steps, unreacted nickel, co-produced cobalt and copper product were eluted with 6 M HCl (30 ml), 4 M HCl (15 ml) and 0.1 M HCl (9 ml), respectively. The ^{64}Cu fraction was delivered to the TADDEO module and evaporated to dryness at 160 °C in 1 h under a constant nitrogen flow, and finally re-dissolved in 400 µl.
To recover the decayed ^{64}Ni, the first fraction was loaded on the AG1-X8 resin, eluted with 6 M HCl (30 ml), evaporated to dryness, re-dissolved in H_2O (20 ml), evaporated to dryness, re-dissolved in ethanol (15 ml) and evaporated to dryness. The residue was retreated with HNO_3 (2 ml, 6 M) and further processed as previously explained, to prepare the electrochemical ^{64}Ni solution.

Characterization
The pH of the copper fraction was determined with a pH meter by Mettler Toledo (Greifensee, Switzerland). All three purification fractions were analysed with gamma spectroscopy (GC2020-CP5SL, Mirion Technologies (former Canberra) GmbH, Rüsselsheim, Germany) with the Gamma Analysis S501 software), to calculate the overall radionuclide composition of the production run and to determine the ^{64}Cu purity. Using an ISOMED 2010 dose calibrator (MED Nuklear-Medizintechnik Dresden GmbH, Dresden, Germany), final product activity and half-life was verified. The specific activity of ^{64}Cu was determined via titration with TETA (1,4,8,11-Tetraazacyclotetradecane-1,4,8,11-tetraacetic acid, from Macrocylics, Dallas, Texas, USA), as presented by McCarthy et al.[19]. A copper stock solution in NH_4OAc (0.1 M, pH 5.5) with a concentration of 10 MBq/30µl was prepared. 0.03 – 0.2 µg of TETA and 10 MBq copper stock solution were diluted in NH_4OAc (300 µl, 0.1 M, pH 5.5) and incubated for 30 min at 37 °C. Radio-TLC was performed on ITLC-SA stripes (Agilent, Waldbronn, Germany) with NaCl (0.9%) as mobile phase (R_f(TETA) = 0.8 - 0.9; R_f(^{64}Cu) = 0.0).
ICP-OES analysis was performed on decayed ^{64}Cu aliquots at the analytical division of the Faculty for Chemistry and Pharmacy, LMU Munich, to determine non-radioactive metallic impurities (Co, Cr, Cu, Fe, Mn, Ni, Zn).

Labelling
The 6A10 Fab was conjugated with *p*-NCS-benzyl-NODA-GA (2,2′-(7-(1-carboxy-(4-(4-isothiocyanatobenzyl) amino)-4-oxobutyl)-1,4,7-triazacyclononane-1,4-diyl) diacetic acid from CheMatech (Dijon, France)) in phosphate buffer (400 µl reaction volume, 0.1 M, pH 8.5) for 1 h at 37 °C. Not complexed chelator was removed using nap-5 columns (GE Healthcare, Munich, Germany). The conjugate was labelled with $^{64}CuCl_2$ in NH_4OAc (500 - 600 µl reaction volume, 0.1 M, pH 5.5) at 37 °C for 20 min followed by a nap-5 column purification. Radio-TLC on ITLC-SA stripes (15 – 95 mm) in citric buffer (pH 4.5) was used for quality control (R_f(Fab) = 0.0 – 0.1; R_f(NODA-GA) = 0.1 - 0.3; R_f (free ^{64}Cu)= 0.1 – 1.0).

PET imaging
The glioma cell line U87MG (American Type Culture Collection) was cultivated in Gibco MEM media by Thermo Fischer Scientific (Munich, Germany), supplemented with Fetal Bovine Serum and L-Glutamine (Biochrom Berlin, Germany) and kept at 5% CO_2 and 37 °C in a CB150 incubator by Binder (Tuttlingen, Germany). $5x10^6$ U87MG cells were subcutaneously injected into the right shoulder of a female SCID-mouse (6-8 weeks, 20-25 g). 14.7 MBq was injected through a tail vein catheter after a tumor growth time of 12 days. Under constant anaesthesia (Isoflurane Vet. Med. Vapor, Drägerwerk, Lübeck) the mouse was scanned 4 h post injection for 70 min (60 min emission and 10 min transmission) on an Inveon P120 µPET scanner (Siemens, Munich, Germany; Inveon acquisition workplace, Siemens Medical Solutions, Knoxville, USA). PET images were analysed with the Inveon Research Workplace software. Region-of-interest (ROI) analysis was performed using a tumor ROI based on 40% threshold (239 µl) and a background ROI (ellipsoid, 100 ml) in the contralateral thigh muscle. Average ROI counts were calculated.All animal experiments were performed in accordance to the current German animal protections laws and protocols of the local authorities.

Keywords: ^{64}Cu • Comecer Alceo • solid target • 6A10 Fab • PET

Conflict of Interest

The authors declare no conflict of interest.

References:

[1] B. J. Hackel, R. H. Kimura, Z. Miao, H. Liu, A. Sathirachinda, Z. Cheng, F. Chin, S. S. Gambhir, *J. Nucl. Med.* **2013**, *54*, 1101 - 1105.

[2] H. Chen, G. Niu, H. Wu, X. Chen, *Theranostics* **2016**, *6*, 78 - 92.

[3] J. Oxboel, M. Brandt-Larsen, C. Schjoeth-Eskesen, R. Myschetzky, H. H. El-Ali, J. Madsen, A. Kjaer, *Nucl. Med. Biol.* **2014**, *41*, 259-267.

[4] P. Bustany, M. Chatel, J. M. Derlon, F. Darcel, P. Sgouropoulos, F. Soussaline, A. Syrota, *J. Neuro-Oncol.* **1986**, *3*, 397-404.

[5] J. W. Hicks, H. F. VanBrocklin, A. A. Wilson, S. Houle, N. Vasdev, *Molecules* **2010**, *15*, 8260-8278.

[6] I. Kayani, J. B. Bomanji, A. Groves, G. Conway, S. Gacinovic, T. Win, J. Dickson, M. Caplin, P. J. Ell, *Cancer* **2008**, *112*, 2447 - 2455.

[7] H. Zhuang, M. Pourdehnad, E. S. Lambright, A. J. Yamamoto, M. Lanuti, P. Li, P. D. Mozley, M. D. Rossman, S. M. Albelda, A. Alavi, *J. Nucl. Med.* **2001**, *42*, 1412 - 1417.

[8] G. W. Severin, J. W. Engle, R. J. Nickles, T. E. Barnhart, *J. Med. Chem.* **2011**, *7*, 389-394.

[9] T. J. Wadas, E. H. Wong, G. R. Weisman, C. J. Anderson, *Chem Rev.* **2010**, *110*, 2858 - 2902.

[10] D. G. Covell, J. Barbet, O. D. Holton, C. D. V. Black, R. J. Parker, J. N. Weinstein, *Cancer Res* **1986**, *46*, 3969-3978.

[11] C. T. Mendler, L. Friedrich, I. Laitinen, M. Schlapschy, M. Schwaiger, H.-J. Wester, A. Skerra, *mAbs - Taylor & Francis* **2015**, 96-109.

[12] R. W. Kinne, K. Schemer, T. Behr, R. M. Sharkey, E. Palombo-Kinne, F. Emmrich, D. M. Goldenberg, F. Wolf, W. Becker, *Nucl. Med. Commun.* **1999**, *20*, 67-75.

[13] C. Wanke, K. Kossert, O. J. Nähle, O. Ott, *Appl. Radiat. Isot.* **2010**, *68*, 1297-1302.

[14] G. Wermann, D. Alber, W. Pritzkow, G. Riebe, J. Vogl, W. Görner, *Appl. Radiat. Isot.* **2001**, *56*, 145-151.

[15] S. M. Qaim, T. Bisinger, K. Hilgers, D. Nayak, H. H. Coenen, *Radiochim. Acta* **2007**, *95*, 67-73.

[16] A. H. Al Rayyes, Y. Ailouti, *World J. Nucl. Sci. Technol.* **2013**, *3*, 72-77.

[17] M. Shokeen, C. J. Anderson, *Acc. Chem. Res.* **2009**, *42*, 832-841.

[18] A. N. Asabella, G. L. Cascini, C. Altini, D. Paparella, A. Notaristefano, G. Rubini, *BioMed Res. Int.* **2014**, *2014*, 1-9.

[19] D. W. McCarthy, R. E. Shefer, R. E. Klinkowstein, L. A. Bass, W. H. Margeneau, S. Cutler, C. J. Anderson, M. J. Welch, *Nucl. Med. Biol.* **1997**, *24*, 35-43.

[20] M. S. Cooper, M. T. Ma, K. Sunassee, K. P. Shaw, J. D. Williams, R. L. Paul, P. S. Donnelly, P. J. Blower, *Bioconjugate Chem.* **2012**, *23(5)*, 1029-1039.

[21] C. J. Anderson, R. Ferdani, *Cancer Biother.Radiopharm.* **2009**, *24*, 379-393.

[22] H. Wang, D. Li, S. Liu, R. Liu, H. Yuan, V. Krasnoperov, H. Shan, P. S. Conti, P. S. Gill, Z. Li, *J. Nucl. Med.* **2015**, *56*, 908-913.

[23] Q. Xie, h. Zhu, F. Wang, M. X., Q. Ren, C. Xia, Z. Yang, *Molecules* **2017**, *22*, 641-650.

[24] J. E. Mortimer, J. R. Bading, J. M. Park, P. H. Frankel, M. I. Carroll, T. T. Tran, E. K. Poku, R. C. Rockne, A. A. Raubitschek, J. E. Shively, D. M. Colcher, *J. Nucl. Med.* **2018**, *59*, 38-43.

[25] A. Čepa, J. Ráliš, V. Král, M. Paurová, J. Kučka, J. Humajová, M. Lázníček, O. Lebeda, *Appl. Radiat. Isot.* **2018**, *133*, 9-13.

[26] K. Lam, C. Chan, R. M. Reilly, *mAbs* **2017**, *9*, 154-164.

[27] L. Y. Kwon, D. A. Scollard, R. M. Reilly, *Mol. Pharmaceutics* **2017**, *14*, 492-501.

[28] L. K. van Dijk, C. B. Yim, G. M. Franssen, J. H. Kaanders, J. Rajander, O. Solin, T. J. Gronroos, O. C. Boerman, J. Bussink, *Contrast Media Mol. Imaging* **2016**, *11*, 65-70.

[29] E. Lucente, H. Liu, Y. Liu, X. Hu, E. Lacivita, M. Leopoldo, Z. Cheng, *Bioconjugate Chem.* **2018**.

[30] S. Sarkar, N. Bhatt, Y. S. Ha, P. T. Huynh, N. Soni, W. Lee, Y. J. Lee, J. Y. Kim, D. N. Pandya, G. I. An, K. C. Lee, Y. Chang, J. Yoo, *J. Med. Chem.* **2018**, *61*, 385-395.

[31] D. Zeng, N. S. Lee, Y. Liu, D. Zhou, C. S. Dence, K. L. Wooley, J. A. Katzenellenbogen, M. J. Welch, *ACS Nano* **2012**, *6*, 5209-5219.

[32] H. Lee, A. F. Shields, B. A. Siegel, K. D. Miller, I. Krop, C. X. Ma, P. M. LoRusso, P. N. Munster, K. Campbell, D. F. Gaddy, S. C. Leonard, E. Geretti, S. J. Blocker, D. B. Kirpotin, V. Moyo, T. J. Wickham, B. S. Hendriks, *Clin. Cancer Res.* **2017**, *23*, 4190-4202.

[33] X. Nie, R. Laforest, A. Elvington, G. J. Randolph, J. Zheng, T. Voller, D. R. Abendschein, S. E. Lapi, P. K. Woodard, *J. Nucl. Med.* **2016**, *57*, 2006-2011.

[34] S. E. Lapi, J. S. Lewis, F. Dehdashti, *Semin. Nucl. Med.* **2015**, *45*, 177-185.

[35] N. Bandara, A. K. Sharma, S. Krieger, J. W. Schultz, B. H. Han, B. E. Rogers, L. M. Mirica, *J. Am. Chem. Soc.* **2017**, *139*, 12550-12558.

[36] A. K. Sharma, J. W. Schultz, J. T. Prior, N. P. Rath, L. M. Mirica, *Inorg. Chem.* **2017**, *56*, 13801-13814.

[37] Q. Jin, W. Zhu, D. Jiang, R. Zhang, C. J. Kutyreff, J. W. Engle, P. Huang, W. Cai, Z. Liu, L. Cheng, *Nanoscale* **2017**, *9*, 12609-12617.

[38] S. Shen, D. Jiang, L. Cheng, Y. Chao, K. Nie, Z. Dong, C. J. Kutyreff, J. W. Engle, P. Huang, W. Cai, Z. Liu, *ACS Nano* **2017**, *11*, 9103-9111.

[39] D. Psimadasa, P. Bouziotisb, P. Georgouliasa, V. Valotassioua, T. Tsotakosb, G. Loudosc, *Contrast Media Mol. Imaging* **2013**, *8*, 333-339.

[40] L. Cheng, S. Shen, S. Shi, Y. Yi, X. Wang, G. Song, K. Yang, G. Liu, T. E. Barnhart, W. Cai, Z. Liu, *Adv. Funct. Mater.* **2016**, *26*, 2185-2197.

[41] W. Guo, X. Sun, O. Jacobson, X. Yan, K. Min, A. Srivatsan, G. Niu, D. O. Kiesewetter, J. Chang, X. Chen, *ACS Nano* **2015**, *9*, 488-495.

[42] H. J. Seo, S. H. Nam, H.-J. Im, J.-Y. Park, J. Y. Lee, B. Yoo, Y.-S. Lee, J. M. Jeong, T. Hyeon, J. Who Kim, J. S. Lee, I.-J. Jang, J.-Y. Cho, D. W. Hwang, Y. D. Suh, D. S. Lee, *Scientific Reports* **2015**, *5*, 15685.

[43] C. Alliot, N. Michel, A.-C. Bonraisin, V. Bossé, J. Laizé, C. Bourdeau, B. M. Mokili, F. Haddad, *Radiochim. Acta* **2011**, *99*, 627-630.

[44] S. Thieme, M. Walther, H.-J. Pietzsch, J. Henniger, S. Preusche, P. Mäding, J. Steinbach, *Appl. Radiat. Isot.* **2012**, *70*, 602-608.

[45] C. M. Jeffery, S. V. Smith, A. H. Asad, S. Chan, R. I. Price, in *AIP Conference, Vol. 1509*, **2012**, pp. 84-90.

[46] M. A. Avila-Rodriguez, J. A. Nye, R. J. Nickles, *Appl. Radiat. Isot.* **2007**, *65*, 1115-1120.

[47] J. Y. Kim, H. Park, J. C. Lee, K. M. Kim, K. C. Lee, H. J. Ha, T. H. Choi, G. I. An, G. J. Cheon, *Appl. Radiat. Isot.* **2009**, *67*, 1190-1194.

[48] M. Matarrese, P. Bedeschi, R. Scardaoni, F. Sudati, A. Savi, A. Pepe, V. Masiello, S. Todde, L. Gianolli, C. Messa, F. Fazio, *Appl. Radiat. Isot.* **2010**, *68*, 5-13.

[49] K. A. Kraus, F. Nelson, in *Proc. Int. Conf. Peaceful Uses At. Energy, Vol. 7*, Geneva, **1956**, pp. 113-131.

[50] C. Battke, E. Kremmer, J. Mysliwietz, G. Gondi, C. Dumitru, S. Brandau, S. Lang, D. Vullo, C. Supuran, R. Zeidler, *Cancer Immunol. Immunother.* **2011**, *60*, 649-658.

[51] G. Gondi, J. Mysliwietz, A. Hulikova, J. P. Jen, P. Swietach, E. Kremmer, R. Zeidler, *Cancer Res.* **2013**, *73*, 6494-6503.

[52] S. Ivanov, S.-Y. Liao, A. Ivanova, A. Danilkovitch-Miagkova, N. Tarasova, G. Weirich, J. Maerrill, M. A. Proescholdt, E. H. Oldfield, J. Lee, J. Zavada, A. Waheed, W. Sly, M. I. Lerman, E. J. Stanbridge, *Am. J. Pathol.* **2001**, *158*, 905-919.

[53] R. M. Torcynski, A. P. Bollon, *Vol. U.S. Patent 5,589,579*, **1996**.

[54] A. J. Kivelä, S. Parkkila, J. Saarnio, T. J. Karttunen, J. Kivelä, A. K. Parkkila, S. Pastoreková, J. Pastorek, A. Waheed, W. S. Sly, H. Rajaniemi, *Histochem. Cell Biol.* **2000**, *114*, 197-204.

[55] Ö. Türeci, U. Sahin, E. Vollmar, S. Siemer, E. Göttert, G. Seitz, A.-K. Parkkila, G. N. Shah, J. H. Grubb, M. Pfreundschuh, W. S. Sly, in *Proc. Natl. Acad. Sci. USA, Vol. 95*, **1998**, pp. 7608-7613.

[56] S. Parkkila, A.-K. Parkkila, J. Saarnio, J. Kivelä, T. J. Karttunen, K. Kaunisto, A. Waheed, W. S. Sly, Ö. Türeci, I. Virtanen, H. Rajeniemi, *J. Histochem. Cytochem.* **2000**, *48*, 1601-1608.

[57] C. C. Wykoff, N. Beasley, P. H. Watson, L. Campo, S. K. Chia, R. English, J. Pastorek, W. S. Sly, P. Patcliffe, A. L. Harris, *Am. J. Pathol.* **2001**, *158*, 1011-1019.

[58] P. Hynninen, L. Vaskivuo, J. H. Saarnio, H., J. Kivelä, S. Pastoreková, J. Pastorek, A. Waheed, W. S. Sly, U. Puistola, S. Parkkila, *Histopathol.* **2006**, *49*, 594-602.

[59] M. A. Proescholdt, C. Mayer, M. Kubitza, T. Schubert, S.-Y. Liao, E. J. Stanbridge, S. Ivanov, E. H. Oldfield, A. Brawanski, M. J. Merrill, *Neuro-Oncol.* **2005**, *7*, 465-475.

[60] L. Fiedler, M. Kellner, A. Gosewisch, R. Oos, G. Böning, S. Lindner, N. Albert, P. Bartenstein, H.-J. Reulen, R. Zeidler, F. J. Gildehaus, *Nucl. Med. Biol.* **2018**, *60*, 55-62.

[61] T. Toyota, T. Hanafusa, T. Oda, I. Koumura, T. Sasaki, E. Matsuura, H. Kumon, T. Yano, T. Ono, *J. Radioanal. Nucl. Chem.* **2012**, 295-300.
[62] A. Obata, S. Kasamatsu, D. W. McCarthy, M. J. Welch, H. Saji, Y. Yonekura, Y. Fujibayashi, *Nucl. Med. Biol.* **2003**, *30*, 535-539.
[63] I. Rose, C. Whittington, Belgium, **2014**.
[64] F. Szelecsényi, G. Blessing, S. M. Qaim, *Appl. Radiat. Isot.* **1993**, *44*, 575-580.
[65] R. Adam Rebeles, P. Van den Winkel, A. Hermanne, F. Tárkányi, *Nucl. Instrum. Methods Phys. Res., Sect. B* **2009**, *267*, 457-461.
[66] J. C. Manrique-Arias, M. A. Avila-Rodriguez, *Appl. Radiat. Isot.* **2014**, *89*, 37-41.
[67] T. Ohya, K. Nagatsu, H. Suzuki, M. Fukada, K. Minegishi, M. Hanyu, T. Fukumura, M.-R. Zhang, *Nucl. Med. Biol.* **2016**, *43*, 685-691.
[68] Data received from Comecer SpA.

Fully automated production and characterization of ^{64}Cu and proof-of-principle small animal PET imaging using ^{64}Cu labelled CA XII targeting 6A10 Fab

Luise Fiedler[a]*, Markus Kellner[b], Rosel Oos[a], Guido Böning[a], Sibylle Ziegler[a] Peter Bartenstein[a], Reinhard Zeidler[b][c], Franz Josef Gildehaus[a], Simon Lindner[a]*

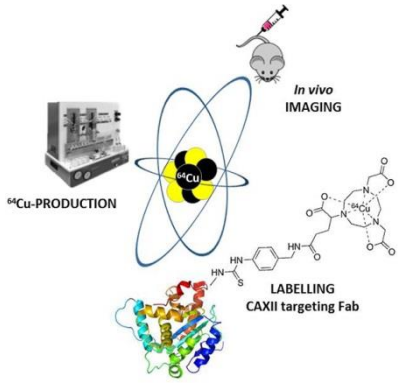

An automated ^{64}Cu production using the first generation Alceo setup was established and evaluated. Volume, pH, radionuclide purity, non-radioactive metal impurities and molar activity of the product were determined. The CA XII targeting 6A10 Fab fragment was radiolabelled with the produced ^{64}Cu and proof-of-principle small animal PET imaging was performed.